Experimental Evidence of a UV Light-Induced Long-Range Electric Field in Nanostructured TiO_2 Thin Films in Contact with Aqueous Electrolytes

T. Lana-Villarreal,[†] J. Bisquert,*[,‡] I. Mora-Seró,[‡] and P. Salvador*[,†,§]

Instituto de Catálisis y Petroleoquímica, CSIC, Madrid, Spain, Departament de Ciències Experimentals, Universitat Jaume I, 12080 Castelló, Spain, and Departamento de Matemáticas e Informática, Universidad de las Islas Baleares, Cra. Valldemosa km 7.5, 07071 Palma, Spain.

Received: January 11, 2005

Nanostructured TiO_2 thin-film electrodes of controlled thickness were obtained by immobilization of TiO_2 powder (Degussa P25) on SnO_2:F (FTO)-coated glasses by electrophoresis. The photocurrent−potential characteristics of the electrodes in contact with an indifferent aqueous electrolyte, for both front- and backside UV illumination, show the existence of a macroscopic electric field in the electrode region near the FTO substrate. This electric field, which is only photoinduced in the presence of water (it does not appear in TiO_2 dye-sensitized solar cells under visible illumination), apparently disappears when an efficient hole scavenger, like methanol, is added to the aqueous electrolyte. It is attributed to a nonhomogeneous spatial accumulation of photogenerated holes at surface-bound OH radicals resulting from the photooxidation of chemisorbed water molecules. The influence of film thickness and UV illumination mode (front- and backside) on the photoinduced electric field is analyzed by solving the transport equations for diffusion and drift of electrons.

1. Introduction

Photoelectrocatalytic degradation of organic pollutants in the presence of titanium dioxide nanoparticles appears to be a viable decontamination method for widespread applications.[1,2] The immobilization of nanoparticles over a conducting support provides important advantages: It eliminates the need for separation of the catalyst and reduces electron−hole recombination by removing photogenerated electrons, thereby improving photodegradation efficiency significantly.[3,4] To have a large surface area, the catalyst film should be as porous as possible. The photoelectrochemical behavior of semiconductor electrodes is well-known.[5,6] In massive titanium dioxide (single-crystal and polycrystalline electrodes), photogenerated electron hole pairs are separated by a macroscopic electric field (band bending) at the interfacial depletion layer.[6] By contrast, in nanoporous semiconductor electrodes consisting of a network of sintered nanosized particles, the electrolyte penetrates all the film, with each particle being in contact with the electrolyte so that a priori, the macroscopic electric field is shielded.[7] Photogenerated holes react with reductant dissolved species within each nanoparticle, while photogenerated electrons migrate by diffusion toward the back contact, recombining partially with holes and/or oxidizing electrolyte dissolved species, like oxygen. Södergren et al.[5] consider the diffusion length of electrons $L = (D\tau)^{1/2}$, where D is the carrier diffusion coefficient and τ is the electron lifetime constant through the film, which means that recombination is a first-order reaction in the concentration of conduction band electrons.

In contact with an aqueous electrolyte, water molecules become adsorbed on the TiO_2 surface, the adsorption behavior depending on the electrolyte pH and on the TiO_2 point of zero charge. Under illumination with photons of energy higher than the band gap, electron−hole pairs are generated. Holes react with adsorbed hydroxyl groups producing surface-bound $OH_s^{\bullet}$ radicals. The accumulation of positive surface charge at $OH_s^{\bullet}$ species produces a shift of the semiconductor band edges toward lower energies.[8] Moreover, the existence of a spatial distribution of $OH_s^{\bullet}$ species induces a long-range electric field component within the film. Experimental evidence about the existence of a macroscopic electric field near the back contact in illuminated nanostructured TiO_2 thin films in contact with aqueous electrolytes has been reported by Boschloo et al.[9] and Levy et al.,[10] although these authors did not refer to its origin.

Here, we analyze the nature of this photoinduced electric field by studying the photocurrent−voltage dependence as a function of the electrode film thickness, d, and the illumination mode (electrolyte or back contact side), in both the absence and presence of an efficient hole scavenger, like methanol, dissolved in the aqueous electrolyte.

2. Experimental Section

Preparation of Nanostructured TiO_2/SnO_2:F Thin-Film Electrodes. Fluoride−tin oxide (FTO) on glass plates (10 Ω per square) were obtained from Solems (France). TiO_2 layers were deposited on the FTO substrate by electrophoresis from a suspension of TiO_2 Degussa P25 (75% anatase, 25% rutile, diameter 20 nm) in methanol (1% w/v).[11,12] A potential of 10 V was applied between the FTO substrate and a platinum counter electrode. TiO_2 films of variable thickness were obtained by controlling the polarization time from 5 to 120 s. The TiO_2 films so obtained were finally annealed at 450 °C for 1 h in air.

Photoelectrochemical Measurements. Photoelectrochemical experiments were performed using a Liconix He−Cd laser with a 325-nm emission line as the illumination source. The intensity of the incident light was measured with an optical power meter

* Corresponding authors: dmipss9@uib.es (P. Salvador), bisquert@uji.es (J. Bisquert).
[†] Instituto de Catálisis y Petroleoquímica.
[‡] Universitat Jaume I.
[§] Universidad de las Islas Baleares.

10.1021/jp050182p CCC: $30.25
Published on Web 05/04/2005

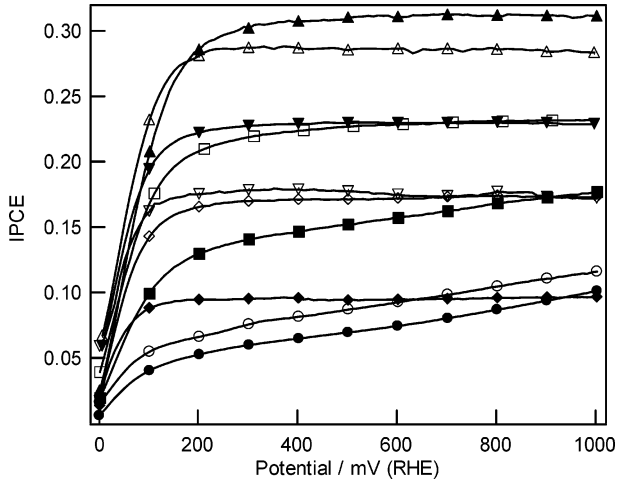

Figure 1. IPCE vs potential curves of nanostructured TiO_2 (Degussa P25)/SnO_2:F electrodes of variable thickness, in contact with N_2-purged 0.5 M H_2SO_4, under EE illumination of 325 nm and a potential scan rate of 20 mV/s. Electrodes (●EP5, ○EP7, ■EP10, □EP15, ▲EP17, △EP20, ▼EP30, ▽EP40, ◇EP60, ◆EP120) where obtained by electrophoresis; the numbers indicate the deposition time.

UDT (model 371) equipped with a head sensor UDT (model 222). The illumination area was about 3 mm^2. Dark- and photocurrent versus potential curves were obtained with a commercial computer-controlled potentiostat (Wenking POS2). A platinum wire was used as the counter electrode and a reversible hydrogen electrode (RHE) as the reference electrode. The photoelectrochemical cell was equipped with a UV light transparent quartz window. Argon gas was bubbled through the electrolyte before and during the experiments in order to remove dissolved oxygen. The electrolyte was prepared with H_2SO_4 (Merck) and ultrapure Millipore Q Water.

3. Results and Discussion

Hereafter, nanostructured TiO_2 film electrodes prepared from TiO_2 P25 aqueous suspensions are designed as EP5, EP10, and so on, with the number indicating the electrophoresis deposition time (see Experimental Section).

Figure 1 shows the incident photon flux to current conversion efficiency (IPCE) versus potential curves as a function of the deposition time (film thickness) under electrolyte−electrode (EE) illumination. Two well-defined regions are observed. For $E \leq 200$ mV (RHE), the IPCE increases smoothly with the applied potential. As far as the deposition time increases and the film becomes thicker, d(IPCE)/dE decreases in the region of $E \geq 200$ mV (RHE). In particular, for deposition times higher than ~15 s, the IPCE becomes potential independent. The IPCE dependence on the deposition time under polarization at 300 mV (RHE) is shown in Figure 2. A maximum IPCE of ~0.3 is obtained for a deposition time of about 17 s. This maximum IPCE can be explained as follows: As the deposition time increases, thicker layers are formed (d increases). If the film is very thin, a part of the incident photons are not absorbed (are not useful for generating electron/hole pairs), so the IPCE decreases. On the other hand, if the film is too thick, electron/hole pairs will be photogenerated too far away from the back contact and their probability of recombination before reaching the back contact increases. This means that a maximum IPCE should be obtained for $d \approx {}^1/_\alpha$, as is the case for sample EP17 with a thickness around 0.7 μm as measured with a step profiler.

The IPCE dependence on the polarization potential for different values of the deposition time under substrate−electrode (SE) illumination is shown in Figure 3. Curiously, the plateau seen in Figure 1 for EE illumination and $E \geq 200$ mV (RHE) is not observed under SE illumination, even for the thickest film. The deposition time (film thickness) dependence of the IPCE under polarization at 400 mV (RHE) and SE illumination is shown in Figure 4. In this case, the IPCE maximum observed in Figure 2 is not observed, with the IPCE reaching a plateau for deposition times greater than 20 s.

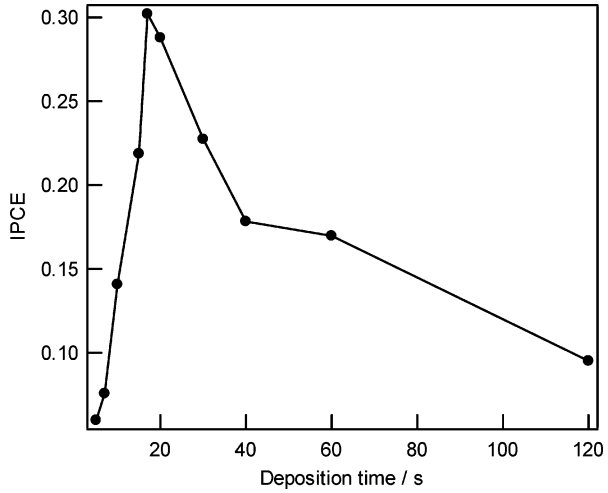

Figure 2. Dependence of the IPCE on the electrophoresis deposition time for nanostructured TiO_2 (Degussa P25)/SnO_2:F electrodes in contact with N_2-purged 0.5 M H_2SO_4, biased at 0.3 V vs RHE, under EE illumination of 325 nm.

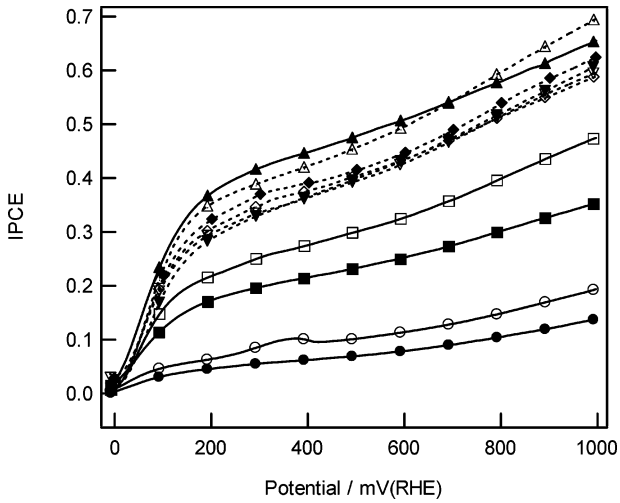

Figure 3. IPCE vs potential curves of nanostructured TiO_2 (Degussa P25)/SnO_2:F electrodes of variable thickness in contact with N_2-purged 0.5 M H_2SO_4, under SE illumination of 325 nm and a potential scan rate of 20 mV/s. The electrodes are the same ones used in Figure 1 (●EP5, ○EP7, ■EP10, □EP15, ▲EP17, △EP20, ▼EP30, ▽EP40, ◇EP60, ◆EP120). IPCE values have not been corrected by glass/SnO_2:F absorption.

Let us define the relative slope (RS) of the IPCE versus E curves in the $E \geq 200$ mV (RHE) region as

$$\mathrm{RS} = 100\,\frac{I_{800} - I_{300}}{I_{800}}$$

where I_{800} and I_{300} are the IPCE values at 800 and 300 mV versus RHE, respectively. Figure 5 shows the RS dependence on the deposition time for both SE and EE illumination. RS decreases as the deposition time (film thickness) increases, reaching a constant value for $d \approx 0.7$ μm (electrode EP17). RS was found to be independent of the potential scan rate.

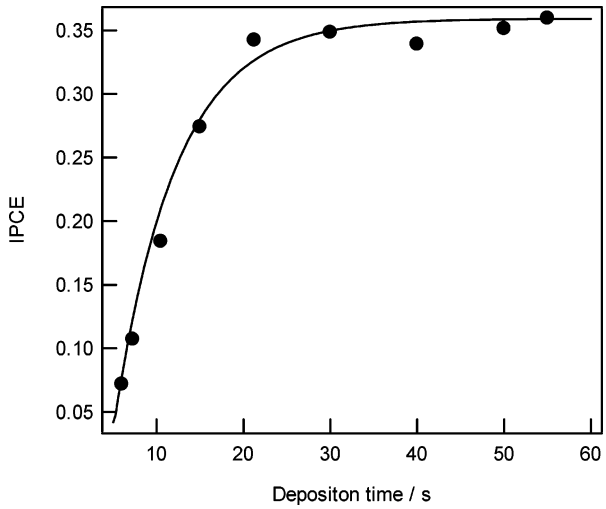

Figure 4. Dependence of the IPCE on the electrophoresis deposition time (electrode thickness) of nanostructured TiO_2 (Degussa P25)/SnO_2:F electrodes in contact with N_2-purged 0.5 M H_2SO_4, biased at 0.3 V vs RHE, under EE illumination of 325 nm.

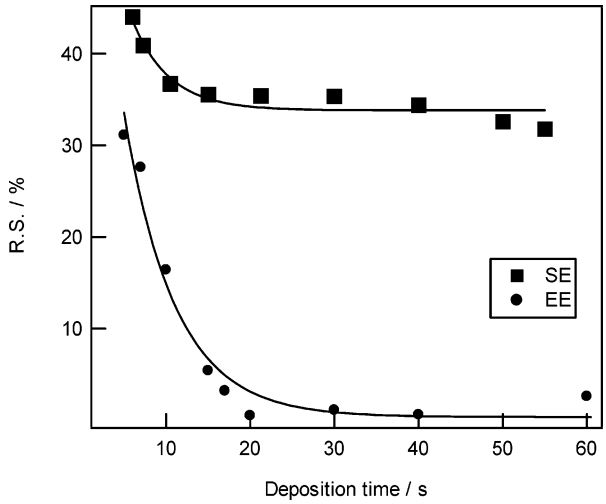

Figure 5. Dependence of the relative slope (RS) of the IPCE vs potential plots of Figures 1 and 3, as defined in the text, on the electrophoresis deposition time.

The addition of an efficient hole scavenger to the aqueous electrolyte, like methanol, produces a drastic decrease in RS under both SE and EE illumination. Figure 6 shows the I_{ph} versus E plot for a thick electrode (EP40), in the presence and absence of dissolved 0.2 M methanol. A drastic decrease of RS in the plateau region is observed. The same behavior is obtained for a similar electrode not annealed (see inset), which demonstrates that it is not due to the formation of a compact polycrystalline layer near the back contact during the thermal treatment.

In summary, the experimental results presented show that under SE illumination the IPCE increases monotonically with the positive applied potential for $E \geq 200$ mV (RHE) (see Figure 3). By contrast, under EE illumination, this monotonic increase of the IPCE only takes place for electrodes of thickness below a critical value $d_c \approx 10^{-4}$ cm (see Figure 1), with d_c being the light penetration length for $\lambda = 325$ nm ($d_c \approx 1/\alpha_{325}$), that is, the inverse of the absorption coefficient of the nanostructured TiO_2 film for the wavelength used in the experiments. This means that under EE illumination the IPCE depends on the applied potential only for those photons absorbed near the back contact. Moreover, the applied potential dependence of the IPCE

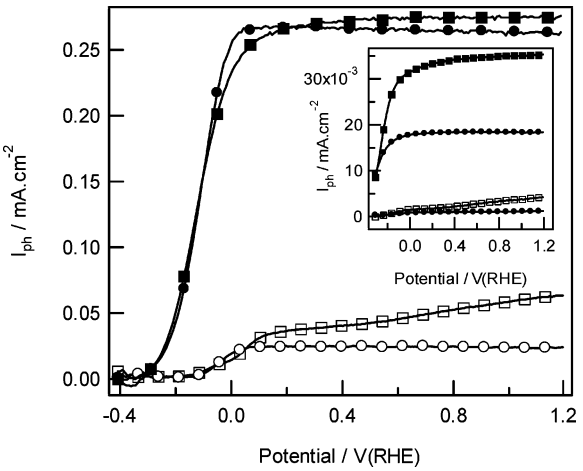

Figure 6. Photocurrent density vs potential curves of the EP40 nanostructured TiO_2 (Degussa P25)/SnO_2:F electrode in contact with N_2-purged 0.5 M H_2SO_4, with (■, ●) and without (□, ○) added 0.2 M methanol, under SE (■, □) and EE (●, ○) illumination of 325 nm (11mW) and potential scan rate of 20 mV/s. I_{ph} values were not corrected by glass/SnO_2:F absorption. The inset corresponds to the same electrode without sintering thermal treatment.

observed under SE illumination disappears when an efficient hole scavenger is added to the electrolyte.

These results suggest the photogeneration of a macroscopic electric field in the electrode region near the back contact, which affects the recombination rate of photogenerated electron−hole pairs and is modified by the applied potential bias. In the following we will show that this electric field is associated with a nonhomogeneous spatial distribution of photogenerated holes trapped as surface-bound $OH_s^{\bullet}$ radicals resulting from the photooxidation of chemisorbed water molecules. We stress that this electrical field is not the origin but the result of charge separation within the nanostructured TiO_2 film, as the separation of photogenerated charge carriers is a consequence of the higher rate of interfacial transfer for holes than for electrons.[13]

The incorporation of a long-range photoinduced electrical field in the conventional transport model, which considers diffusion as the only driving force, leads to a nonlinear equation system where the electrical field depends on the carrier distribution and, therefore, on the electron transport rate. The drift and diffusion contribution to electron transport can be obtained by solving this nonlinear system of equations. This will help to explain the experimental photocurrent density dependence on the applied bias and the influence of the electrode thickness.

Electric shielding conditions in nanostructured TiO_2 electrodes have been amply discussed in relation to dye-sensitized solar cells (DSSC).[14,15] It is widely accepted that under equilibrium conditions in the dark an electric field appears within a thin region near the substrate, with the TiO_2 bands considered to be flat. Under illumination and/or applied potential bias, a long-range electrical field (absent in equilibrium) is consistent with a short-range screening.[16] On the other hand, it has been claimed that the charging of surface states in TiO_2 DSSC generates an electric field contributing to the drift mobility of electrons.[17,18] Note that in DSSC electrons are generated only via direct injection from photoexcited, adsorbed dye species. The accumulation of positive electrolyte ions at the TiO_2−electrolyte interface generates a band shift no higher than 0.15 eV[19] so that the drift contribution to electron mobility can be considered to be negligible and the major driving force for electron transport is due to diffusion.

In our SnO_2-TiO_2 aqueous electrolyte system, photogenerated electron−hole pairs are generated under UV illumination, with holes being rapidly trapped as surface-bound $OH_s^\bullet$ radicals, producing a surface accumulation of positive charge which leads to a potential drop at the Helmholtz layer[8]

$$\Delta\varphi = e\frac{\Delta[OH_s^\bullet]}{c_H} \tag{1}$$

where e is the positive elementary charge, $[OH_s^\bullet]$ is the surface concentration of surface-bound $OH_s^\bullet$ radicals, and c_H is the Helmholtz capacitance. Here, c_H is the specific Helmoltz capacitance per microscopic surface unit; the specific Helmoltz capacitance per volume unit is defined as $C_H = pc_H$, where p (cm^{-1}) is the internal surface-to-volume ratio. For an electrode composed of particles of radius r and void fraction f_v, it is $p = (4\pi r^3/3)^{-1}(4\pi r^2)(1 - f_v) = 3(1 - f_v)/r$. Associated with $\Delta\varphi$ exists a change of electrostatic energy of electrons, which is given by the shift of the lower conduction band edge, E_c ($\Delta E_c = -e\Delta\varphi$). Consequently, a gradient of $[OH_s^\bullet]$ produces an electrical field in the direction normal to the substrate, of which the intensity is

$$F = -\frac{\partial\varphi}{\partial x} = -\frac{e}{c_H}\frac{\partial[OH_s^\bullet]}{\partial x} \tag{2}$$

The incorporation of a macroscopic field F due to a position-dependent potential drop at the Helmholtz layer is frequent in transport models used in electrochemistry of porous metal electrodes and batteries.[20,21] This macroscopic electrical field, which appears under illumination nonequilibrium conditions, is consistent with overall charge neutrality, because the surface charge associated with surface-bound photogenerated $OH_s^\bullet$ radicals at each nanoparticle is balanced by the electrolyte charge accumulated in the outer Helmholtz plane. Because the conductivity of the electrolyte is very high, charge transport in the electrolyte needs not be considered by the model.

To complete our model we need to specify the rate of the interfacial reactions involving photogenerated electrons and holes, which must be coupled to the diffusion−migration equation through the conservation equation, as usually done in standard electrochemical models involving current and potential distributions in porous electrodes.[20,21]

To calculate the spatial distribution of photogenerated electrons, $n(x)$, holes, $p(x)$, and $OH_s^\bullet$ radicals, $[OH_s^\bullet](x)$, we consider that the following set of reactions takes place[22]

$$TiO_2 + h\nu \xrightarrow{\upsilon_0} h^+ + e^- \qquad \upsilon_0 = \alpha\Phi_0 e^{-\alpha x}$$

$$h^+ + OH_s^- \xrightarrow{\upsilon_1} OH_s^\bullet \qquad \upsilon_1 = k_1 p(x)[OH_s^-](x)$$

$$OH_s^\bullet + e^- \xrightarrow{\upsilon_2} OH_s^- \qquad \upsilon_2 = k_2[n(x) - n_0][OH_s^\bullet](x)$$

$$OH_s^\bullet + RH_2 \xrightarrow{\upsilon_3} OH_s^- + RH^\bullet + H^+ \qquad \upsilon_3 = k_3[RH_2][OH_s^\bullet](x) \tag{3}$$

which describe electron−hole pair generation, hole capture at surface-bound OH^- species, electron−hole recombination via photogenerated surface-bound $OH^\bullet$ radicals, and removal of surface-trapped holes via interfacial transfer to RH_2 (hole scavengers) electrolyte dissolved species, respectively.

At the steady state the reaction rates obey the conditions

$$\upsilon_0 = \upsilon_1 \tag{4}$$

$$\upsilon_1 = \upsilon_2 + \upsilon_3 \tag{5}$$

so that

$$[OH_s^\bullet](x) = \frac{\alpha\Phi_0 e^{-\alpha x}}{k_2[n(x) - n_0] + k_3[RH_2]} \tag{6}$$

Moreover, the conservation equation for electrons takes the form[23]

$$-\frac{\partial J(x)}{\partial x} + \alpha\Phi_0 e^{-\alpha x} - k_2[n(x) - n_0][OH_s^\bullet](x) = 0 \tag{7}$$

with the electron flux being

$$J_n = -D_n\frac{\partial n}{\partial x} - \frac{eD_n(n - n_0)}{k_B T}F \tag{8}$$

The photoinduced electric field associated with the accumulation of surface-bound $OH_s^\bullet$ can be calculated from eqs 2 and 6. By substituting the value of F into eq 8, the following expression for the electron flux toward the back contact is obtained

$$J_n = -D_n\frac{\partial n}{\partial x} - \frac{e^2 D_n(n - n_0)}{k_B T c_H}\frac{\alpha\Phi_0 e^{-\alpha x}}{k_2(n - n_0) + k_3[RH_2]} \times \left[\alpha + \frac{k_2}{k_2(n - n_0) + k_3[RH_2]}\frac{\partial n}{\partial x}\right] \tag{9}$$

The boundary conditions under EE illumination are

$$n(x = d) = n_0 \tag{10}$$

$$J(x = 0) = 0 \tag{11}$$

and under SE illumination

$$n(x = 0) = n_0 \tag{12}$$

$$J(x = d) = 0 \tag{13}$$

where d is the layer thickness and $x = 0$ is positioned at the illuminated layer interface in each case. Equations 7 and 9 have been solved numerically by employing the fourth-order Runge−Kutta method. The electron distribution and the electron flux collected at the substrate are then calculated. The shooting method has been used to transform the initial conditions into a problem with boundary conditions.

The electron concentration is related to the Fermi level, E_F, by the expression

$$n = N_c \exp\left[\frac{(E_F - E_c)}{k_B T}\right] \tag{14}$$

where k_B is the Boltzmann constant, T is the temperature, and N_c is the effective density of states in the conduction band. The

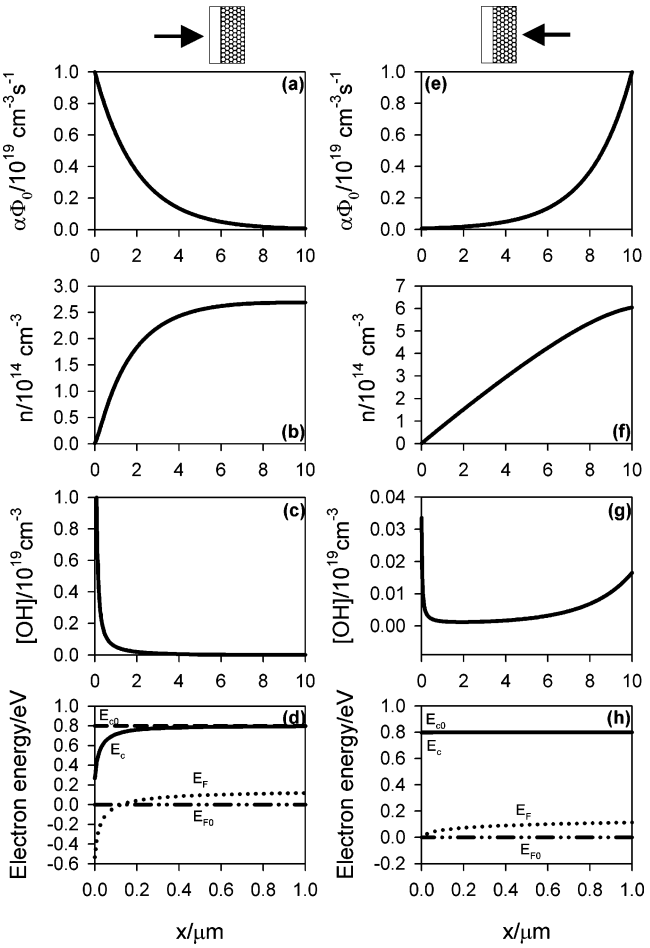

Figure 7. Calculated values of (a, e) photogeneration profile, (b, f) electron concentration profile, (c, g) surface-bound photogenerated $OH_s^•$ radicals concentration profile, and (d, h) electron energy profile including the quasi-Fermi level (E_F) and conduction band (E_c), corresponding to a nanostructured semiconductor electrode 10-μm thick composed of 10-nm-radius nanoparticles (void factor $f_v = 0.5$), in contact with the aqueous electrolyte under SE illumination and polarization at 0.53 V (a, b, c, d) or EE illumination and short-circuit conditions (e, f, g, h). The back contact is situated at $x = 0$. Intervening parameters: $\alpha = 5 \times 10^3$ cm^{-1}, $n_0 = 10^{12}$ cm^{-3}, $D_n = 10^{-5}$ cm^2/s, $c_H = 10$ μF/cm^2, $p = 1.5 \times 10^6$ cm^{-1}, $\Phi_0 = 2 \times 10^{15}$ cm^{-2} s^{-1}, $k_2 = 10^{-13}$ cm^3 s^{-1}, $k_3[RH_2] = 0.1$ s^{-1}, $E_{C0} - E_{F0} = 0.8$ eV (difference under equilibrium dark conditions). Ten thousand integration steps were used in the calculations.

applied potential V has two components:

$$V = V_F + V_{BS} \tag{15}$$

The term V_F due to the modification of the Fermi level can be written

$$V_F = -k_B T \ln\left(\frac{n}{n_0}\right) \tag{16}$$

where n and n_0 are the electron concentrations at the contact, both under illumination and under equilibrium conditions in the dark, respectively (eqs 10 and 12); the term V_{BS}, representing the conduction band shift associated with hole accumulation at the TiO_2/substrate interface, is given by eq 1.

Let us interpret the experimental results in light of this model. The behavior predicted by the model under strong enough polarization potential is shown in Figure 7 for both SE (left side) and EE (right side) illumination. The electron distribution (Figure 7b,f) results from the photogeneration term (Figure 7a, e). The $[OH_s^•]$ distribution (Figure 7c,g) and the energy diagram (Figure 7d,h) are calculated from eqs 1, 6, 14, and 16. Equation 9 indicates that the drift contribution contains two terms, both pushing electrons toward the back contact, because $\partial n/\partial x$ is positive near the substrate (see Figure 7b,f). Figure 7d clearly shows the existence of a macroscopic electric field extending up to about 0.4 μm inside the film from the back contact. Finally, Figure 7h indicates that the band shift near the substrate practically disappears under EE illumination, as the $[OH_s^•]$ gradient far away from the substrate significantly decreases (Figure 7g).

Let us first consider the origin of the different shapes of the experimental IPCE versus potential curves of Figures 1 and 3. Figure 8 shows the result of the numerical simulations. For a better understanding of the effect of the band shifts in the interpretation of the experimental results, calculated IPCE versus potential curves under EE and SE illumination are shown in Figure 8a and 8b, respectively. Both voltage components of eq 15(V_F and V_{BS}) are taken into account. As can be seen in Figure 8a, the contribution of the band shift term, V_{BS}, associated with the accumulation of photogenerated surface-bound OH• radicals (Fermi-level displacement with respect to conduction band, V_F) is very small under EE illumination, in qualitative agreement with the experimental results of Figure 1. By contrast, the effect of the V_{BS} term on the IPCE versus potential plots under SE illumination is significant (the potential region where IPCE increases before attaining the plateau broadens up to about 1.2 V in Figure 8b, just the effect observed in the experimental results of Figure 3). Moreover, it must be emphasized that, in general, diffusion is the main driving force for electron transport toward the substrate. The broadening of the potential region where the IPCE increases is also present under EE illumination for thin enough films (Figure 8c), as the accumulation of positive charge associated with photogenerated surface-bound $OH_s^•$ radicals near the contact is also high because of the weak absorption of photons by the thin electrode. The addition of an efficient hole scavenger (RH_2) to the electrolyte produces a drastic decrease of $[OH_s^•]$ and, therefore, of $\Delta\varphi$ (eq 1) so that the band shift contribution term (V_{BS}) in eq 15 practically disappears, resulting in a situation analogous to that observed under EE illumination (Figure 8d), in agreement with the experimental results of Figure 6.

Let us finally discuss the experimental IPCE dependence on the electrode thickness shown in Figures 2 and 4. According to the model, under short circuit conditions and SE illumination (Figure 8f) electron−hole pairs are photogenerated near the contact independently of the electrode thickness so that electrons are able to leave the electrode easily (small recombination); consequently, the IPCE does not depend on the electrode thickness above a critical value $d_c \approx {}^1/_\alpha$ for which incident photons are fully absorbed by the electrode. This is, in fact, the experimental behavior observed in Figure 4. By contrast, under EE illumination (Figure 8e), electron−hole pairs are generated in the opposite side of the contact so that the probability for recombination before electrons attain the contact increases with the electrode thickness, and an IPCE decrease is produced. On the other hand, if the electrode is thin enough ($d < d_c \approx 1/\alpha_{325}$), incident photons are not fully absorbed and the IPCE diminishes so that a maximum value of IPCE appears for $d \approx d_c$, in agreement with the experimental results of Figure 2.

4. Conclusions

The factors governing transport and extraction of electrons at illuminated TiO_2 nanostructured electrodes in contact with

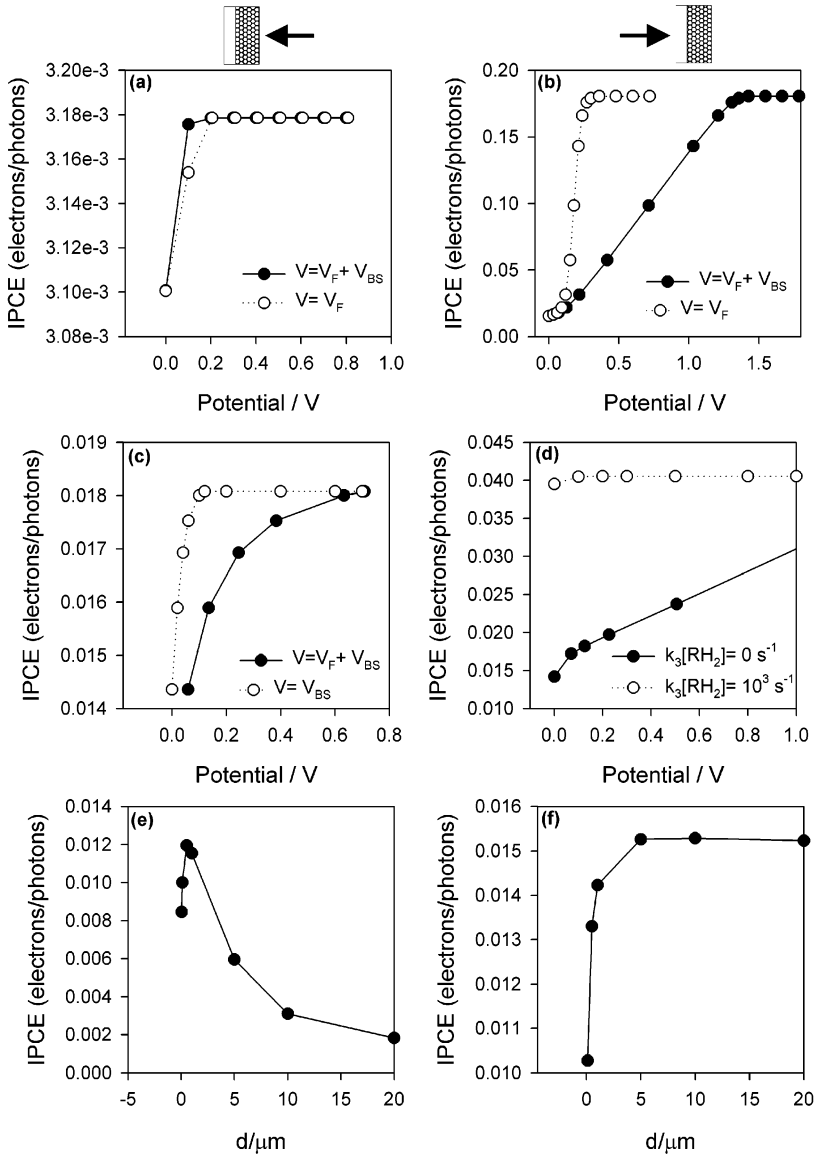

Figure 8. Calculated IPCE dependence on the applied potential (a, b, c, d) and film thickness under short-circuit conditions (e, f) for a nanostructured electrode under EE illumination (a, c, e) or SE illumination (b, d, f). The influence of adding a hole scavenger to the aqueous electrolyte for $k_3[RH_2] = 0\ s^{-1}$ and $k_3[RH_2] = 10^3\ s^{-1}$ is shown in d. Common intervening parameters: $\alpha = 5 \times 10^3\ cm^{-1}$, $d = 1\ \mu m$, $r = 10$ nm, $n_0 = 10^{12}\ cm^{-3}$, $D_n = 10^{-5}\ cm^2/s$, $c_H = 10\ \mu F/cm^2$, $p = 1.5 \times 10^6\ cm^{-1}$, $\Phi_0 = 2 \times 10^{15}\ cm^{-2}\ s^{-1}$, $k_3[RH_2] = 0\ s^{-1}$, $f_v = 0.5$, $k_2 = 10^{-10}\ cm^3\ s^{-1}$. Particular parameters: $k_2 = 10^{-12}\ cm^3\ s^{-1}$ for a, b, and c; $k_3[RH_2] = 0.1\ s^{-1}$ and $d = 10\ \mu m$ for f. Ten thousand integration steps were used in the calculations.

aqueous electrolytes have been analyzed. Under illumination from the substrate side (SE illumination), a position-dependent band shift (macroscopic electric field) is generated near the substrate because of the accumulation of a positive charge distribution associated with photogenerated surface-bound $OH_s^{\bullet}$ radicals. Although this photoinduced, macroscopic electric field does not contribute significantly to the extraction of electrons via a drift mechanism, its effect on the potential dependence of the IPCE becomes significant. On the other hand, when thick enough electrodes are illuminated from the electrolyte side (EE illumination), surface-bound $OH_s^{\bullet}$ radicals are photogenerated far away from the back contact and no electric field appears in the near contact region; therefore, the applied potential does not affect the IPCE. The effect of adding an efficient hole scavenger to the aqueous electrolyte is to drastically reduce the concentration of photogenerated surface-bound $OH_s^{\bullet}$ radicals so that the electric field photoinduced near the back contact under SE illumination practically disappears and the IPCE dependence on the applied potential becomes negligible, as for EE illumination.

Acknowledgment. T. Lana Villarreal acknowledges the Ministerio de Educación y Ciencia of Spain for a Ph.D. fellowship. This work was partially supported by the EC under project contract ICA3-CT-1999 00016 and by MEyC under project MAT2004-05 168.

Glossary

c_H = specific Helmholtz layer capacitance per unit of real surface area.

C_H = specific Helmholtz capacitance per volume unit.

D = electron diffusion coefficient.

d = electrode thickness.

d_c = critical electrode thickness ($d_c = {}^1/_\alpha$).

DSSC = dye-sensitized solar cell.

e = positive elementary charge.

E_c = conduction band edge.
E_F = Fermi-level position.
EE = electrolyte−electrode illumination.
F = electric field intensity.
f_v = void fraction.
FTO = fluorinated tin oxide.
I_{300} = IPCE at 300 mV vs RHE.
I_{800} = IPCE at 800 mV vs RHE.
IPCE = incident photon flux-to-current conversion efficiency.
J = electron flux.
k_1 = hydroxyl radical generation rate constant.
k_2 = recombination rate constant.
k_3 = indirect photooxidation rate constant.
k_B = Boltzmann constant.
L = electron diffusion length.
n = electron density under illumination.
n_0 = electron density at equilibrium in the dark.
N_c = effective density of states in the conduction band.
$OH_s^{\bullet}$ = surface-bound hydroxyl radicals.
p = internal surface-to-volume ratio or surface hole density.
r = particle radius.
RH_2 = dissolved hole scavenger.
RHE = reversible hydrogen electrode.
RS = relative slope.
SE = substrate−electrode illumination.
T = temperature.
α = absorption coefficient.
Φ_0 = incident light intensity.
φ = potential drop at the Helmholtz layer.
τ = electron lifetime.

References and Notes

(1) Hoffman, M. R.; Martin, S. T.; Choi, W.; Bahnemann, D. W. *Chem. Rev.* **1995**, *95*, 69.

(2) Mills, A.; Le Hunte, S. *J. Photochem. Photobiol., A: Chem.* **1997**, *108*, 1.

(3) Fernández-Ibáñez, P.; Malato, S.; Enea, O. *Catal. Today* **1999**, *54*, 329.

(4) Butterfield, I. M.; Christensen, P. A.; Hammet, A.; Shaw, K. E.; Walker, G. M.; Walker, S. A.; Howarth, C. R. *J. Appl. Electrochem.* **1997**, *27*, 385.

(5) Södergren, S.; Hagfeldt, A.; Olsson, J.; Lindquist, S. E. *J. Phys. Chem.* **1994**, *98*, 5552.

(6) Morrison, S. R. *Electrochemistry at Semiconductor and Oxidized Metal Electrodes*; Plenum Press: New York, 1980.

(7) O'Regan, B.; Moser, J.; Anderson, M.; Grätzel, M. *J. Phys. Chem.* **1990**, *94*, 8720.

(8) Salvador, P. *J. Phys. Chem.* **1985**, *89*, 3863.

(9) Boschloo, G. K.; Gossens, A.; Schooman, J. *J. Electroanal. Chem.* **1997**, *428*, 25.

(10) Levy, B.; Liu, W.; Gilbert, S. E. *J. Phys. Chem. B* **1997**, *101*, 1810.

(11) Byrne, J. A.; Eggins, B. R.; Brown, N. M. D.; McKinney, B.; Rouse, M. *Appl. Catal., B* **1998**, *17*, 25.

(12) Zhitomirsky, I. *Adv. Colloid Interface Sci.* **2002**, *97*, 279.

(13) Hodes, G.; Howell, I. D. J.; Peter, L. M. *J. Electrochem. Soc.* **1992**, *139*, 3136.

(14) Zaban, A.; Meier, A.; Gregg, B. A. *J. Phys. Chem. B* **1997**, *101*, 7985.

(15) Bisquert, J.; Garcia-Belmonte, G.; Fabregat Santiago, F. *J. Solid State Electrochem.* **1999**, *3*, 337.

(16) Bisquert, J.; Cahen, D.; Hodes, G.; Rühle, S.; Zaban, A. *J. Phys. Chem. B* **2004**, *108*, 8106.

(17) Vanmaekelbergh, D.; de Jongh, P. E. *J. Phys. Chem. B* **1999**, *103*, 747.

(18) Bisquert, J. *J. Phys. Chem. B* **2004**, *108*, 2323.

(19) Schlichthörl, G.; Huang, S. Y.; Sprague, J.; Frank, A. J. *J. Phys. Chem. B* **1997**, *101*, 8141.

(20) Newman, J. S.; Tobias, C. W. *J. Electrochem. Soc.* **1962**, *109*, 1183.

(21) Bisang, J. M.; Jüttner, K.; Kreysa, G. *Electrochim. Acta* **1994**, *39*, 1297.

(22) Lana Villareal, T.; Gómez, R.; Neumann-Spallart, M.; Alonso-Vante, N.; Salvador, P. *J. Phys. Chem. B* **2004**, *108*, 15172.

(23) Mora-Seró, I.; Lana Villarreal, T.; Bisquert, J.; Pitarch, A.; Gómez, R.; Salvador, P. *J. Phys. Chem. B* **2005**, *109*, 3371.